Transcriptomic profiling of mouse amygdala during opioid dependence and withdrawal by single-cell RNA sequencing

Yan Yan
University of Miami Miller School of Medicine
Bridget Herlihy
University of Miami Miller School of Medicine
Sean Boyles
University of Miami Miller School of Medicine
Junyi Tao
University of Miami https://orcid.org/0000-0003-2638-5386
William Hulme
University of Miami Miller School of Medicine
Sabita Roy (Sabita.Roy@miami.edu)
University of Miami Miller School of Medicine

Resource

Keywords:

Posted Date: April 11th, 2022

DOI: https://doi.org/10.21203/rs.3.rs-1299708/v1

Transcriptomic profiling of mouse amygdala during opioid dependence and withdrawal by single-cell RNA sequencing

Yan Yan[1], Bridget Herlihy[1], Sean Michael Boyles[2], Junyi Tao[1], William Hulme[2], Sabita Roy[1*]

[1]Department of Surgery, [2]John P. Hussman Institute for Human Genomics, University of Miami Miller School of Medicine, Miami, FL 33136, USA

* Corresponding Author

Correspondence:
Sabita Roy, Ph.D.
1501 NW 10th Ave, BRB 531
Miami, FL 33136
Phone: (305) 243-8452
Email: Sabita.Roy@miami.edu

Abstract

Substance use disorder (SUD) is a complex process in which several neurocircuits are disturbed and various brain regions are involved. The amygdala is a region that mediates the withdrawal effect as well as anxiety and depression-like behaviors. However, the specific transcriptional changes in each cell type during SUD is largely unknown. Here we performed single-cell RNA sequencing and classified all cell types in mouse amygdala under opioid dependence and withdrawal conditions. Our data revealed key biological processes, such as immune response, inflammation, synaptic transmission, and mitochondrial respiration, changed in a distinct manner in different cell populations. Dramatic differences were unraveled in the transcriptional profiles between dependence and withdrawal states. Overall, our work has provided a comprehensive dataset of genes, biological pathways and cell-cell interactions for all the identified cell types in the amygdala, thus expanding our limited understanding of brain alterations during SUD, especially at the molecular and cellular levels.

Introduction

Prevalence of substance use disorder (SUD) and associated deaths [1] have spurred efforts to develop new strategies for prevention or treatment of SUD. This requires us to gather better understandings of brain alterations during this complex, multistage process. It is well known that SUD is characterized by disturbances in several major neurocircuits that are driven by different brain regions: basal ganglia-driven intoxication stage, amygdala-driven withdrawal stage, and prefrontal cortex-driven anticipation stage [2]. However, the alterations of these brain regions at the molecular and cellular levels remain largely unknown. Previous studies applying bulk tissue preparations [3-6] have provided meaningful insights into SUD, but these data represented the changes in a mixture of cell populations; thus, the cell type-specific information was not unraveled. Yet, this information is highly important for us to understand the heterogenous brain and to discover novel therapies that target specific genes/pathways in a specific cell population. Advances of the single-cell RNA sequencing (scRNA-seq) technology has enabled us to study thousands of cells belonging to different cell types simultaneously. A few studies have applied scRNA-seq to investigate different brain regions in SUD, including the nucleus accumbens (NAc) after acute morphine treatment [7], and the prefrontal cortex (PFC) during cocaine addiction [8]. Yet, the amygdala which mediates the negative effect during drug withdrawal [2] and modulates emotions such as anxiety and depression that occur as co-morbidities of SUD [9, 10], has not been studied before.

In this study, we analyzed the transcriptomic profiles of 77,957 individual cells from mouse amygdala. Distinct gene expression changes in different cell types under morphine dependence and withdrawal conditions were revealed. Our data suggests key biological processes and pathways are modulated in a cell-type specific manner following morphine dependence. Notably, dramatic changes of the cellular status were observed when the brain underwent morphine withdrawal. We also investigated cell-cell communications under dependence and withdrawal states by analyzing ligand-receptor interactions that were modified under these two conditions. Overall, our current work has provided a comprehensive dataset of genes, biological pathways and ligand-receptor interactions for all the identified cell types in the amygdala. This data will provide insight into our limited understanding of how the brain behaves during SUD, especially at the molecular and cellular levels. This study will also provide clues to develop novel preventative and therapeutic strategies for SUD.

Results

Identification of cell types in the amygdala

To study the mouse brain under different conditions of SUD, mice were treated with morphine sulphate for 7 days to induce dependence. In the withdrawal studies, morphine injection was stopped at day 7 for 24 hours to induce spontaneous withdrawal (Supplementary Fig. 1a). As expected, the mouse body weight was reduced after morphine treatment (Supplementary Fig. 1b), and consistent with the withdrawal condition the mice exhibited withdrawal symptoms such as jumping and wet dog shaking (Supplementary Fig. 1c). We dissected the amygdalae from the naïve (Naive), morphine dependent (Dep), and morphine withdrawal (With) mouse

brains, after which the tissues were dissociated to single cell suspension. The cells were captured with the 10X Chromium platform, and the scRNA-seq was conducted to examine the transcriptomic profiles (Fig. 1a).

We sequenced 121,856 cells from 9 independent biological samples, each of which was derived from pooled amygdalae of 4 to 5 mice in a single treatment group. We removed debris, dead cells, potential doublets and unrecognized clusters (see Methods). In the end, our analysis resulted in 77,957 high quality cells, representing 17 cell types (Fig. 1b), with distinct expression profiles (Fig. 1c, 1d). As shown in Fig. 1e, with a higher number of cells being captured and analyzed, the number of detected genes in the cell population was increased, and it was in the stem cell/precursor cell types (NSC, NRP, OPC) that we observed a higher average number of genes/UMI counts per cell.

The proportion of each cell type was consistent among the three experimental groups (Supplementary Fig. 2f, 2g). Although the estimated percentages might not reflect the actual composition of the amygdala since different cell types have different sensitivity to the dissociation procedure, these data suggested that the tissue composition of the amygdala remained unchanged after chronic morphine treatment. The sequencing metrics such as median UMI per cell and the average number of detected genes were also consistent among the three groups (Supplementary Fig. 3). Other metrics are summarized in Supplementary Table 2.

Identification of differentially expressed genes under morphine dependence and withdrawal conditions

We then studied the transcriptional changes in each cell type under the morphine dependence condition (Dep vs. Naive), and under the withdrawal condition following the dependence status (With vs. Dep), by analyzing the differentially expressed genes (DEG). In both comparisons, each cell type exhibited distinct changes (Fig. 2a, 2b, Supplementary Fig. 4-5, Supplementary Table 4-5). Under the dependence condition, there were more upregulated genes than downregulated genes in NEUR, EC, OPC and MG (Fig. 2c). Compared to the dependence condition, the numbers of DEG under the withdrawal condition were almost doubled in most of the cell types (Fig. 2d), suggesting that there were more dramatic changes in the amygdala when the brain switched from morphine dependence to withdrawal.

Among the cell populations, neurons showed the highest numbers of DEG under both conditions: there were 859 downregulated and 1058 upregulated genes under dependence (Fig. 2e), while over 4000 genes were differentially expressed between the withdrawal and dependence status (Fig. 2f). As the resident immune cells, microglia showed distinct changes (Fig. 2h, 2i). When we investigated the overlapping relation between these DEG under two conditions, we found that around 60% and 45% of the DEG under the dependence state were inversely changed under the withdrawal state in NEUR (Fig. 2g) and MG (Fig. 2j) respectively. However, these inverse DEG counted for only a small percentage (~30% in both NEUR and MG) of the DEG in the withdrawal state.

Next, we studied the DEG that were shared across cell types. Interestingly, heat shock protein genes were on top of the DEG list (Supplementary Table 4-5). Therefore, we analyzed the changes of the genes encoding heat shock proteins in 17 cell types. As shown in Fig. 2k, in most glia cell types Hsp90 family genes were downregulated, while the Hsp70 family (*Hspa1a*, *Hspa1b*) and Hsp40 family genes were upregulated under the dependence condition. But when these cells were undergoing withdrawal, these heat shock proteins were mostly downregulated (Fig. 2l). Since heat shock proteins play important roles in protein folding and stress response [11], these data revealed how brain cells responded to the stresses that were induced by either chronic opioid treatment or opioid withdrawal.

Validation of cell type specific gene expression changes

Next, we sought to validate some of the cell type specific DEG by mRNA fluorescence in situ hybridization (FISH). As discussed before, some of the heat shock proteins such as *Dnaja1* showed distinct changes under the morphine dependence and withdrawal conditions (Fig. 2k, 2l, 3a). This was confirmed in microglia cells (*Temem119*$^{+}$) as shown in Fig. 3b, 3c. In addition, we observed that the number of *Dnaja1* mRNA puncta was generally increased under dependence while decreased under the withdrawal condition in other cells (*Temem119*$^{-}$) in the amygdala. This observation verified our single-cell data showing that the changes of *Dnaja1* were shared by several glia cell populations (Fig. 2k, 2l).

Ccl2 is one of the most potent microglia chemokines that attract cells involved in the immune or inflammatory response. Consistent with our single-cell data (Fig. 3d), the independent FISH data showed that *Ccl2* mRNA expression was induced in the microglia cells with chronic morphine treatment but was reduced following 24-hour morphine withdrawal (Fig. 3e, 3f).

Morphine dependence and morphine withdrawal induced distinct pathway changes in neurons and microglial cells

Next, we conducted a gene set enrichment analysis (GSEA) [12] to investigate the changes of various gene sets or pathways in each cell population. We first focused on neurons which showed the highest number of DEG. Under the dependence condition, among the 4497 biological process gene ontology terms (GOs) that were analyzed, 802 GOs were significantly upregulated while 6 GOs were downregulated (Supplementary Table 9). We then constructed an enrichment map [13] of the most significantly changed GOs. As shown in Fig. 4a, the synaptic transmission GOs such as trans-synaptic signaling, neurotransmitter transport, glutamatergic transmission, were upregulated. Correspondingly, the GOs that were related to synaptic transmission, including protein/ion transport, synaptic plasticity, etc. were also activated. Various metabolic processes and cellular respiration were promoted, which could provide more building blocks and energy to support the increased neuronal activity. When we compared the withdrawal neurons to the dependent cells, there were 942 upregulated and 581 downregulated GOs (Supplementary Table 10). The enrichment map (Fig. 4b) showed further activation of the macromolecule metabolic processes and gene expression. However, there was a decrease in synaptic transmission with the relevant GOs significantly deactivated. This was

associated with reduced nucleotide metabolism and cellular respiration. Interestingly, these withdrawal neurons exhibited an activated immune response, and various cytokine production pathways were also promoted.

Microglia, as the resident immune cells in the brain, play a pivotal role in the immune response and neuroinflammation [14]. Their activity is linked to various emotions and behaviors such as compulsive behaviors, anxiety, depression, and SUD [15-18]. Our GSEA data showed that 1143 biological process GOs were significantly changed (947 upregulated, 196 downregulated) under morphine dependence, while there were more deactivated GOs (468 upregulated, 1026 downregulated) when comparing the withdrawal state to dependence (Supplementary Table 9 and 10). Consistent with our current understanding of opioid induced neuroinflammation [15, 19, 20] and microglia activation during opioid treatment [21, 22], in the morphine dependent microglia, the cell activation pathways were enhanced and the immune response, inflammatory response, cytokine production as well as the response to cytokines were promoted (Fig. 4c). The pathways involved in metabolic processes and gene expression were also activated. In agreement with the literature [21, 23, 24], our data showed that chronic opioid treatment resulted in microglia apoptosis, and enhanced MAPK as well as ERK pathways. However, as shown in Fig. 4d, under the withdrawal condition these activated pathways were mostly downregulated, suggesting a dramatic switch of the cellular status when the brain underwent the withdrawal process. Importantly, cellular responses to stress including the immune response, response to ROS, protein folding, etc. were deactivated, which was consistent with our DEG analysis showing a dramatic decrease in the expression of the heat shock protein families under the withdrawal condition (Fig. 2l).

Distinct pathway changes were revealed across different cell types

GSEA is more sensitive than the DEG analysis because it aggregates information from a set of genes which are functionally relevant, therefore we were able to conduct GSEA in all the cell types including the populations that had limited cell numbers and didn't show many DEG. Under both dependence and withdrawal conditions, there were shared and cell type-specific changes of gene sets across the 17 cell types (Supplementary Table 9 and 10). Here we compared the GO terms that represented the key biological processes between different conditions (Fig. 4e). With chronic morphine treatment the upregulated translation process and peptide biosynthesis were shared in ASC, MG, OPC, EC, and OLG. Cellular respiration pathways were activated in ASC, OPC, NEUR and NFOLG. Biosynthesis of different molecules and various cell signaling pathways exhibited distinct changes among 17 cell types. As shown here (Fig. 4e-left) and discussed before, MG was the major cell type that increased the immune/inflammatory response and cytokine production under dependence.

Compared to these dependent cells, the withdrawal cells showed more dramatic changes (Fig. 4e-right). Gene expression GOs were downregulated in almost all the major cell types except neurons. The deactivated cellular respiration pathways occurred not only in NEUR, but also in glia cells (ASC, OPC, MG, EC, OLG, PC). Interestingly, two groups of cell types showed opposite changes in the immune related GOs: EC and immune cell types - MG, MAC, DC, exhibited downregulation; while NEUR, OLG, NFOLG and EPC showed upregulations (discussed later). In

addition, neurotransmitter transport was enhanced in MG, OPC, EC, NFOLG, DC and EPC, but was deactivated in NEUR and PC.

Immune response and inflammation showed distinct and dramatic changes in a cell type specific manner

Among the biological processes being analyzed, immune response related pathways showed the most intriguing changes (Fig. 4). Neuroinflammation is shown to be involved in various neurodegeneration diseases and neuronal disorders such as anxiety and SUD [6, 25, 26]. So next we analyzed the detailed GO terms and pathways that were relevant to the immune response and inflammation. As shown in Fig. 5a-left, when we compared the morphine dependent cells to naïve cells, most of the pathway activations occurred in MG.

More interesting and unexpected changes happened under the withdrawal condition (Fig. 5a-right) when these cell populations could be divided to two groups based on their immune status changes: group1 cell types (MG, MAC, DC, EC) showed deactivations, yet group2 cell types (NEUR, OLG, NFOLG, EPC) showed largely upregulations. The downregulated innate immune response, humoral immune response, inflammatory response, response to cytokines, and TNF production were shared in all the group1 cell types. For other gene sets, MG, DC and EC showed more similar changes. The group2 cell types shared the upregulated immune response and cytokine productions, especially IL6 and interferon gamma production. The inflammatory response and TNF production were enhanced in most of these cell types.

Next, we checked the changes of inflammation related genes. As shown in Fig. 5b, chronic morphine treatment induced the expression of *Ccl2*, *Cx3cl1*, *Gls*, *Tlr4*, *Tnf* in the three immune cell populations – MG, MAC, and DC. Cell types EC and MAC showed a significant upregulation of *Icam1* and *Vcam1*, both of which encoded intercellular adhesion proteins that regulate immune cell recruitment to the sites of inflammation.

Under the withdrawal condition, the group1 immune cells showed decreased expression of *Nlrp3*, *Tlr4*, *Tnf, Hmox1* and several CC chemokine family members. *Icam1* and *Vcam1* expression were reduced in EC. However, the group2 cells exhibited mostly the opposite changes (Fig. 5d). For example, CC chemokine family members (*Ccl12*, *Ccl2*, *Ccl4*) and glutamate metabolism genes (*Gls*, *Glul*) were upregulated in NFOLG and EPC. The induced expression of *Cx3cr1*, *Cxcl12*, *Tnf*, etc*.,* were shared in group2 cell types. Of note, an upregulation of Csf1 receptor was reported in neurons after brain injury and Csf1r signaling facilitated neuron survival [27]. With the upregulation of *Csf1r* shown in NEUR in our data (Fig. 5d), this suggests that under morphine withdrawal the activity of neurons might be dampened, and this was also supported by our data showing cellular respiration and synaptic transmission were significantly decreased in the withdrawal neurons (Fig. 4b).

Cell-cell communications after chronic morphine treatment

Finally, we analyzed the cell-cell interactions (CCI) among all the recognized cell types in the amygdala (see Methods). Based on the DEG analysis, we were able to study the changes of

ligand-receptor/signaling interactions with chronic morphine treatment. Under the morphine dependence condition, we highlighted the communications among NEUR, MG, EC and ASC. As shown in Fig. 6, the increased expression of *Tnf* in MG possibly enhanced the interactions between MG and NEUR, or MG and EC through a variety of receptors or pathways in NEUR or EC. Importantly, this same ligand might regulate different biological processes, depending on the receptors. For example, MG-*Tnf* interacted with several receptors on NEUR (Fig. 6a) and one of them was *Lifr* which was shown to regulate neuron differentiation and maturation [28]. At the same time, *Tnf* upregulation in MG was able to induce the *Csf1* expression in EC (Fig. 6c), and the increased EC-*Csf1* further communicated with several pathways in MG (Fig. 6d), one of which was mediated by the Csf1 receptor (*Csf1r*) that was important for microglial viability and activity [29]. EC also used other ligands to send the signals back to MG. The significantly upregulated *Vcam1* and *Spp1* in EC might potentiate the recruitment of MG to the inflammatory site through binding to the increased receptor *Itga9* on MG (Fig. 6d).

In addition to the CCI between different cell types, our single-cell data also revealed CCI within the same cell type. BDNF, one of the neurotrophin family of growth factors, played pivotal roles in neural growth, survival, plasticity and importantly, it was involved in mood modulation and drug addiction [30, 31]. Our current analysis showed that the increased *BDNF* expression in NEUR, not only promoted its interactions with a variety of receptors on MG (Fig. 6b) and ASC (Supplementary Fig. 8b), but also activated its downstream signaling within the neuron population itself (Supplementary Fig. 8a).

Cell-cell communications under morphine withdrawal

Under the withdrawal condition, a dramatic change was observed in CCI when compared to the dependence state (Fig. 7, Supplementary Fig. 9). Most of the activated interactions between MG and EC under the dependence condition were downregulated (Fig. 7a, 7b). Various cytokine-receptor mediated interactions were reduced between MG and EC, which might contribute to the dampened inflammatory responses in both MG and EC under the withdrawal condition. The signals that MG received, and decreased MG activation were also coming from NEUR. Both the reduced *Cxcl10* in EC (Fig. 7b) and reduced *Cx3cl1* in NEUR (Supplementary Fig. 9a) would possibly deactivate the Ccrl2 mediated pathway in MG, which was important for microglial activation and polarization [32].

Oligodendrocytes produce myelin sheaths that provide support and insulation to neurons, and ependymocytes play pivotal roles in cerebrospinal fluid homeostasis and brain metabolism. Our CCI analysis revealed OLG-NEUR and EPC-NEUR interactions that may also regulate neuron growth and the immune response. As shown in Fig. 7c, 7d and Supplementary Fig. 9c, the increased expression of ligands including *Vtn*, *Fn1*, and *Spp1* in OLG, EPC and NFOLG would enhance their interactions with the receptor *Itga8*, which was also significantly increased in NEUR and was involved in neurite outgrowth [33]. Several cytokine receptors (*Il1rap*, *Cx3cr1*, *Il6ra*, etc.) were upregulated in NEUR, and their corresponding ligands (*Il1a*, *Cxcl10*, *Il6*, etc.) were expressed at increased levels in OLG and EPC; therefore, the interactions between these ligands and receptors most likely will promote immune response in NEUR. Notably, since the cytokine productions were reduced in MG, DC and EC under morphine withdrawal (Fig. 5a, 5c),

the enhanced cytokine signals that NEUR received might mainly come from the non-immune glia cells OLG and EPC.

In summary, our single-cell data unraveled gene expression and pathway changes that regulated key biological processes within each cell population and in other cell types via the modified cell-cell communications.

Discussion

SUD is a complex process in which various brain regions are involved. The amygdala is a recognized region that mediates the withdrawal effect as well as anxiety and depression-like behaviors, both of which are well known co-morbidities of SUD [2, 9, 10]. In this study, we performed scRNA-seq to identify the cell types in mouse amygdala and investigated their unique transcriptional profiles under both morphine dependence and withdrawal states.

As was observed in other scRNA-seq studies investigating the whole brain and other brain regions [7, 8, 34], the mouse amygdala also showed rich cellular heterogeneity. Our study identified 17 major cell types (Fig. 1b), and subtypes for neurons and astrocytes (Supplementary Fig. 6, 7). The proportion of each cell type was consistent, suggesting chronic morphine treatment did not influence the composition of the amygdala tissue, but did affect the transcriptional profiles of all cell types according to our subsequent DEG analysis.

When we compared the morphine dependence sample to the naïve sample, different cell types exhibited distinct transcriptional changes (Fig. 2a, 2e, 2h, Supplementary Fig. 4). When the condition switched to withdrawal, most of the cell populations showed more significant DEG (Fig. 2d), in which neurons exhibited the most prominent changes, suggesting dramatic transcriptional changes in the amygdala after the acute 24-hour morphine withdrawal. These data were in line with the study showing that the transcriptional changes in the PFC neurons were more dramatic during cocaine withdrawal than that during the drug maintenance phase [8]. These imply the importance of the cellular response to withdrawal-induced stimuli in the development of drug dependence.

Heat shock proteins play important roles in protein folding and cellular response to stress [11]. Hsp70 and Hsp40 families were largely upregulated under the morphine dependence condition (Fig. 2k), which was consistent with other studies showing that morphine exposure induced the expression of Hsp70 and Hsp40 mRNAs in various brain regions such as the frontal cortex and amygdala [35, 36]. Considering the role of Hsp70 in cell survival, the function of Hsp40 as the co-chaperone for Hsp70 and their interactions with the MAPK signaling pathways [37, 38], it is likely that the upregulation of these heat shock proteins reflects a protective effect against morphine-induced cell toxicity which has been reported by other research groups [23, 24]. This is also illustrated in our single-cell data with the increased cell death and activated MAPK as well as ERK signaling in glia cells, like microglia (Fig. 4c). In addition, our current data (Fig. 2l) and data by Ammon et. al showed the induced Hsp70 and Hsp40 were reversed under spontaneous withdrawal or by naloxone-precipitated withdrawal [36]. Future studies on the dynamic changes of these heat shock proteins will reveal more information about how the cells respond to stresses under different states in SUD.

Based on the DEG, we conducted GSEA to investigate how different cell types modulated their biological processes. Our data not only revealed findings that were consistent with the literature, but also unraveled novel findings of the cellular status in SUD. Here we highlighted the immune/inflammation process which has been shown to influence neuronal activity and was linked to various neuronal disorders, such as anxiety, depression and SUD [6, 25, 26]. Under morphine dependence, microglia was the major cell type mediating an augmented neuroinflammation, demonstrated by the increased cell activation, enhanced immune and inflammatory responses, promoted cytokine production, etc. (Fig. 4c). Importantly, our data studying the amygdala, which is mainly involved in the negative effect and emotional dysregulation during withdrawal, suggested these dependence-associated changes might be closely related to, or function as, priming events to influence the response to drug withdrawal.

More dramatic and unexpected changes were observed under the morphine withdrawal condition. In this study, we applied a spontaneous withdrawal model that mimics human activity. Therefore, our withdrawal data will complement other studies using precipitated withdrawal models and provide new information into the current understanding of the drug withdrawal process. One of the most recent studies on rat amygdala [39] using laser capture microdissection showed that inflammatory genes, such as *Tnf* and *Il6*, remained unchanged with morphine treatment, yet were upregulated in neurons, microglia and astrocytes in the naltrexone-precipitated withdrawal state. Although our scRNA-seq data didn't show a similar trend in astrocytes, our data did show that *Tnf*, *Icam1*, and *Cxcl12* were upregulated in neurons, and their immune response was activated under the spontaneous withdrawal condition (Fig. 5a, 5d). More importantly, in our data neurons and oligodendrocytes were suggested to be the main cell types that mediate neuroinflammation during spontaneous morphine withdrawal since the immune/inflammatory response in microglia, macrophage, and endothelial cells were downregulated (Fig. 5a). This bidirectional regulation of the immune response in morphine withdrawal is noteworthy. The reduced immune function in the immune cells was possibly due to the absence of morphine, and/or that their cellular activities (immune response is their main function) were compromised as a result of cell death induced by chronic morphine treatment, and/or the signals received from other cells (Fig. 7b). At the same time, the reduced immune response in immune cells might directly or indirectly activate the immune response in neurons and oligodendrocytes, such as by enhancing the expressions of chemokines including *Icam1* and *Cxcl12* to recruit more functional leukocytes. Yet, the synaptic transmission in neurons was greatly affected (Fig. 4b), which would influence the behaviors and emotions during morphine withdrawal. A recent study by Duan et al. showed mitochondria in the amygdala was impaired by chronic stress and mitochondrial loss induced weakening of synapses which resulted in increased anxiety [40]. High-anxious rats exhibited reduced mitochondrial function in the NAc [41]. In our single-cell data, decreased cellular respiration and mitochondrial function were observed in several cell populations, especially in neurons (Fig. 4a and 4e). This suggests that mitochondrial dysfunction in the amygdala might greatly affect neurotransmission during withdrawal and as a result promote anxiety-like behavior that accompanies SUD.

In addition to studying the biological processes in each cell type, we analyzed intercellular communications by measuring the ligand-receptor interactions. This is highly important for studies of the brain since the communications between and within neurons and glia cell types

play pivotal roles in modulating neuronal activity. Especially when we consider the importance of cytokines in immune/inflammatory response, and the link between neuroinflammation and drug dependence/addiction. This cell-cell interaction information will help us to discover novel sources and targets of signal transductions that underly SUD and related co-morbidities.

Our work, as well as recent studies [7, 8, 34], benefited from the sensitivity and power of scRNA-seq to study the highly heterogenous brain tissues and more importantly to investigate cellular changes under different conditions, including drug addiction [7, 8]. Yet, we also encountered the common technical limitations of scRNA-seq, such as the shallow depth of sequencing, the potential sampling problems due to manual and enzymatic dissociation of the brain tissues that might induce differences between experimental groups, etc. Additionally, several limitations of our current study can be improved in future studies, including having single time point of data collection following withdrawal. Future studies aimed at including multiple later time points following morphine withdrawal will allow us to delineate the trajectory analysis. This will also provide more insight into anxiety or depression-like behaviors which occur several days or weeks after drug withdrawal [42, 43]. It will also be useful to optimize our current single cell dissociation protocol (see Methods) to preserve more neurons and oligodendrocytes. The proportion of NEUR and OLG cell types in our single-cell data are lower than that in other scRNA-seq datasets [7, 8, 34, 44]. Although these studies were done with the whole brain or other brain regions and different tissue dissociation procedures were followed, it will be important to explore the ideal protocol so that the scRNA-seq data reflect the actual tissue composition. In the future, it will be meaningful to investigate the subregions in the amygdala considering their different roles in drug withdrawal and anxiety [45]. This might be achieved with spatial transcriptomics [46].

In summary, our current work has provided a comprehensive dataset of genes, biological pathways and ligand-receptor interactions for all the identified cell types under both morphine dependence and withdrawal conditions. As a resource for the neuroscience community and to those who study the biology of drug dependence/addiction, our study not only provides more evidence to support the current understanding, yet in a cell-type specific manner, but also provides novel insight into how different cell populations behave and communicate under different conditions at the molecular level. Since other brain disorders such as anxiety and depression occur during SUD, our data also provide meaningful information in these fields. Last, the novel findings that are revealed in our data provide clues for future strategies targeting either the genes or pathways in specific cell populations for the prevention or treatment of drug addiction and related neuronal disorders.

Methods

Animals

Eight-week-old C57BL/6J male mice were purchased from Jackson Laboratories (Bar Harbor, ME, USA) (https://www.jax.org/strain/003752). Animal maintenance and procedures were conducted according to the Institutional Animal Care and Use Committee policies at the University of Miami. Mice were injected with morphine sulfate (15mg/kg) intraperitoneally (IP)

twice daily (every 12 hours) for 7 days. Mice in the Dep group were sacrificed 3 hours after last injection and mice in the With group were sacrificed 24 hours after last injection. The detailed drug treatment plan was shown in Supplementary Fig. 1a.

Withdrawal behavior test

Withdrawal behavior was monitored 24 hours after the last morphine injection to evaluate both the presence and severity of withdrawal symptoms. Mice were placed in a plexiglass chamber for 15 minutes and their behavior was recorded on a video camera. The videos were scored and verified by a blind observer for withdrawal symptoms that were described previously [47]. In this study, symptoms of withdrawal were evaluated on the frequency of symptoms including wet dog shaking (shaking of head or the entire body), jumping (raising all four paws off the ground rapidly) and grooming (using limbs to manipulate head or body). This resulted in a quantifiable score of the withdrawal symptoms, in which a higher withdrawal score signified higher severity of withdrawal. These withdrawal scores were compared between the With and Naive groups.

Tissue dissociation and single-cell RNA sequencing

Three batches of experiments were conducted, and each batch included one Naive, Dep and With group. Thus, nine independent biological samples were processed. Amygdala dissection and tissue dissociation were performed at the same time period (10am–12pm) for all the samples to limit circadian variation. The widely used Papain Dissociation System (Worthington Cat No. LK003182) was modified based on other published protocols [8, 34] so that single cell solutions with high cell viability (~90%) could be acquired within 2 hours. Briefly, after mice were sacrificed brains were immediately dissected and transferred into ice-cold HBSS. The amygdalae were dissected from 4~5 mice according to the previous protocol [48] and were pooled together. The tissues were cut into small pieces and incubated in 2ml pre-warmed papain solution (EBSS containing approximately 20 units/ml papain and 0.005% DNase) at 30°C for 45 min with gentle constant agitation. After the incubation, all the following procedures were performed on ice. The mixture was triturated gently with a fire polished 2ml Pasteur glass pipette and the supernatant were transferred carefully to a fresh tube. 2ml of EBSS containing the albumin ovomucoid inhibitor was added to the remaining tissues, which was triturated gently with another fire polished 2ml Pasteur glass pipette and the supernatant was transferred. This step was repeated one more time. The resulted 6ml supernatant containing single cells were pooled together and the cell clusters/tissue debris were removed by serial filtration through prewetted 70μm and 40μm cell strainers. The single cell suspension was centrifuged at 220g for 7 min at 4°C. The cells were then washed in 10ml PBS containing 0.04% BSA twice, after which the cells were resuspended in PBS containing 0.04% BSA. 10μl aliquots were stained with Trypan Blue and cell numbers were counted three times for each sample. During the whole procedure, 5% (w/v) trehalose (Sigma Aldrich Cat No. T0167) was added in the buffers to ensure higher cell viability [49].

After dissociation, cell suspensions were diluted to 1,000~1,200 cells/μl with PBS containing 0.04% BSA. For every sample, 16,500 cells were loaded into a Chromium Single Cell 3' Chip (10X Genomics) and processed according to the manufacturer's protocol. scRNA-seq libraries were prepared with the Chromium Single Cell 3' GEM, Library & Gel Bead kits v3.1 (10X Genomics). Libraries were pooled and sequenced on the NovaSeq6000 instrument (Illumina).

Raw data processing and clustering

Cell Ranger (v.6.1) (10X Genomics) was used to perform de-multiplexing, barcode processing and generate the single cell gene expression matrix with the default parameters.

Initial processing and visualization of the scRNA-seq data were performed with the Seurat (v.4.0) package [50, 51] in R (v.4.1). Our initial dataset with nine samples together contained 121,856 cells. For initial quality-control, we filtered the cells with the following parameters: maximum percentage of mitochondrial RNA = 20% (to remove potential dead cells), minimum number of nFeature_RNA = 250 and minimum number of nCount_RNA = 500 (to remove debris), maximum number of nFeature_RNA = 6,000 and maximum number of nCount_RNA = 30,000 (to exclude potential doublets and outliers). We also removed any genes that were only expressed in fewer than 5 cells. With the remaining 82,528 cells we did an initial clustering. To minimize potential batch effect and to perform comparative scRNA-seq analysis across experimental conditions, we applied the Seurat integration procedure [52]. Briefly, the data from each sample were log normalized and scaled to 10,000 transcripts per cell, and the function FindVariableGene() was used to identify variable features for each sample independently. The function SelectIntegrationFeatures() was then used to select features that are repeatedly variable across samples, after which the anchors were identified using the FindIntegrationAnchors() function. Then these anchors were used to integrate the nine samples together with the function IntegrateData(). The integrated data was scaled to find the top 30 principal components (PCs) which were used to identify cell clusters by using the function FindNeighbors() followed by FindClusters() with the resolution as 1.0. This procedure resulted in 46 clusters and the color-coded clusters were visualized with the UMAP plot (Supplementary Fig. 2a).

To determine the cell types for these initial 46 clusters, we first used the function FindAllMarkers() to search for the top differential markers for each cluster, which were then paired with multiple cell-type specific/enriched marker genes (described in the next section). The clusters being assigned to the same cell type were combined and 22 clusters were generated, including two unrecognized clusters (Supplementary Fig. 2b). As the transcriptional profiles shown in Supplementary Fig. 2c, one of the unrecognized clusters expressed both astrocyte marker (*Gja1*) and oligodendrocyte marker (*Mbp*) and the other expressed both neuron marker (*Syt1*) and microglial marker (*Tmem119*). These clusters were likely doublet artifacts arising from the co-capture of multiple cells in one droplet, yet it was also possible they were novel cell types that have not been identified. It will be interesting to investigate these cells in future studies. For our current data analysis, we removed these two clusters. Additionally, we filtered out the cells that belong to meningeal tissue that we didn't remove at the initial dissection step for the sake of fast sample processing. These cells included epithelial

cells (EPIC), arachnoid barrier cells (ABC) as well as vascular and leptomeningeal cells (VLMC) (Supplementary Fig. 2a, 2b). Finally, 77,957 cells representing 17 clusters (Fig. 1b, Supplementary Table 3) with data for 23,057 genes were retained in our dataset for subsequent analysis. For the final dataset, the average number of detected genes, number of UMI counts and percentage of mitochondrial RNA were 2,407.8, 6,508.1, and 9.27% respectively. Other sequencing metrics about each sample, experiment group, batch, and cluster were summarized in Supplementary Table 2, and shown in Supplementary Fig. 2 and 3.

Determination of cell identity

Cell-type specific/enriched marker genes that have been described before to determine cell identity were used: *Gja1* [44] for ASC, *Pdgfra* [53] for OPC, *Tmem119* [54] for MG, *Cldn5* [55] for EC, *Syt1* [56] for NEUR, *Cldn11* [52] and *Mobp* [8] for OLG, *Pf4* [57] for MAC, *Vtn* [58] for PC, *Enpp6* [59] for NFOLG, *Acta2* [54] for VSMC, *Cd74* and *Cd209a* [60] for DC, *Ccdc153* [61] for EPC, *Thbs4* [62] for NSC, *Cd44* [63] for ARP, *Top2a* and *Cdk1* [34] for NRP, *Cd3d* for Tcells, *S100a9* [59] for NEUT, *Ttr* [64] for EPIC; *Slc6a13* [34] for VLMC; *Slc47a1* [34] for ABC. For the neuron and astrocyte sub-clustering, the similar procedures were conducted, and the identification of their subtypes was based on reported neuron [8, 34, 64] or astrocyte [65] subtype marker genes respectively.

Analysis of differentially expressed genes (DEG)

To identify the DEG compared between experiment groups (Dep vs. Naive, With vs. Dep), we used the edgeR (v.3.32) package [66] in R (v.4.1). edgeR generates logFC (with the base as 2), P value and FDR. Specifically, we used the edgeRQLFDetRate method which is based on quasi-likelihood F-test, resulting in more conservative and rigorous type I error rate control [67], and has been shown to perform better than other methods for DEG analysis in scRNA-seq data [68]. With this method we were able to detect significant subtle transcriptional changes in the clusters that had large number of cells, while in relatively small cell populations it was more conservative to identify the DEG with much higher fold changes (Fig. 2a, 2b, Supplementary Table 4 and 5).

Pathway analysis and enrichment map

Gene Set Enrichment Analysis (GSEA) [12] was used to analyze the changes of biological processes or pathways between experiment groups (Dep vs. Naive, With vs. Dep). We used the GSEA software (v.4.1) that was developed and maintained by UC San Diego and Broad Institute [12, 69]. Pathway analysis and visualization were conducted following the protocol described by Reimand et. al [70]. Briefly, for each comparison between experiment groups a ranked gene list was generated for each cell population. These ranked gene lists were used as input, and two databases (GeneOntology and Reactome) were used as references for the GSEA analysis. 1000 permutations were performed. Only gene sets with p value < 0.05 and FDR q value < 0.25 were considered as significantly enriched. Normalized Enrichment Score (NES) was used for

examining gene set enrichment. A positive NES indicated upregulation while negative NES indicated downregulation.

Pathway network visualization was carried out with the EnrichmentMap application (v.3.3) [13] in Cytoscape software (v.3.9). Only the gene sets (p value < 0.05 and FDR q value < 0.15) for GO biological processes were mapped. Pathways were shown as nodes that were connected with edges if the pathways shared many genes. Nodes were colored by NES, and edges were sized on the basis of number of genes shared by the connected pathways. Nodes were manually laid out to form a clearer picture. Gene sets that represented the similar pathways were grouped together and labeled using the AutoAnnotate application (v.1.3) [71]. Individual gene set labels were removed for clarity.

Analysis of cell-cell interactions

The cell-cell communication mediated by ligand-receptor interactions were analyzed using the CCInx (v.0.5) package [34] in R (v.4.1). The ligand-receptor interaction dataset is available at https://baderlab.org/CellCellInteractions. To study the changes of these interactions under morphine dependence or withdrawal conditions, the DEG being analyzed by edgeR were used to build the networks between cell types. In these networks, ligands or receptors in the denoted cell type were represented by the nodes which were colored by the log2FC. Node borders indicated the FDR value of the DEG. Edges represent ligand-receptor interactions. Edge color indicated the sum of scaled differential expression magnitudes from the ligand node and receptor node.

RNAscope in situ hybridization

RNAscope in situ hybridization was performed on fresh-frozen brain tissue from 15 mice (5 Naive, 5 Dep and 5 With). Brains were harvested immediately after the mice were sacrificed. The coronal section (~2mm) containing the amygdala were flash-frozen in OCT (Tissue Tek) and were saved at -80°C until further processing. 14µm coronal sections were cut at -20°C. Multi-channel fluorescence in situ hybridization was performed using the RNAscope Multiplex Fluorescent Manual Assay kit (Advanced Cell Diagnostics (ACD)) following the manufacturer's protocol. Regions of the amygdala were selected according to the Allen Mouse Brain Atalas (https://portal.brain-map.org). Probes against *Tmem119* (ACD Cat No. 472901), *Ccl2* (ACD Cat No. 311791) and *Dnaja1* (ACD Cat No. 454351) were used.

References

1. Jones, C. M., Einstein, E. B. & Compton, W. M. Changes in synthetic opioid involvement in drug overdose deaths in the United States, 2010–2016. JAMA 319, 1819–1821 (2018).

2. Koob, G. F. & Volkow, N. D. Neurobiology of addiction: a neurocircuitry analysis. Lancet Psychiatry 3, 760-773 (2016).

3. Albertson, D. N., Schmidt, C. J., Kapatos, G. & Bannon, M. J. Distinctive profiles of gene expression in the human nucleus accumbens associated with cocaine and heroin abuse. Neuropsychopharmacology 31, 2304-2312 (2006).

4. Korostynski, M., Piechota, M., Kaminska, D., Solecki, W. & Przewlocki, R. Morphine effects on striatal transcriptome in mice. Genome Biol. 8, R128 (2007).

5. Piechota, M. et al. The dissection of transcriptional modules regulated by various drugs of abuse in the mouse striatum. Genome Biol. 11, R48 (2010).

6. Seney, M. L. et al. Transcriptional alterations in dorsolateral prefrontal cortex and nucleus accumbens implicate neuroinflammation and synaptic remodeling in opioid use disorder. Biol. Psychiatry 90, 550-562 (2021).

7. Avey, D. et al. Single-cell RNA-seq uncovers a robust transcriptional response to morphine by glia. Cell Rep. 24, 3619-3629 (2018).

8. Bhattacherjee, A. et al. Cell type-specific transcriptional programs in mouse prefrontal cortex during adolescence and addiction. Nat. Commun. 10, 4169 (2019).

9. Kranzler, H. R. & Liebowitz, N. R. Anxiety and depression in substance abuse: clinical implications. Med. Clin. North. Am. 72, 867-885 (1988).

10. Neighbors, B., Kempton, T. & Forehand, R. Co-occurrence of substance abuse with conduct, anxiety, and depression disorders in juvenile delinquents. Addict. Behav. 17, 379-386 (1992).

11. Miller, D. J. & Fort, P. E. Heat shock proteins regulatory role in neurodevelopment. Front. Neurosci. 12, 821 (2018).

12. Subramanian, A. et al. Gene set enrichment analysis: a knowledge-based approach for interpreting genome-wide expression profiles. Proc. Natl Acad. Sci. USA 102, 15545–15550 (2005).

13. Merico, D., Isserlin, R., Stueker, O., Emili, A. & Bader, G. D. Enrichment Map: A network-based method for gene-set enrichment visualization and interpretation. PloS One 5(11), e13984 (2010).

14. Sara Bachiller, S. et al. Microglia in neurological diseases: a road map to brain-disease dependent-inflammatory response. Front. Cell Neurosci. 12, 488 (2018).

15. Cahill, C. M. & Taylor, A. M. Neuroinflammation-a co-occurring phenomenon linking chronic pain and opioid dependence. Curr. Opin. Behav. Sci. 13, 171-177 (2017).

16. Tränkner, D. et al. A microglia sublineage protects from sex-linked anxiety symptoms and obsessive compulsion. Cell Rep. 29, 791-799 (2019).

17. Stein, D. J., Vasconcelos, M. F., Albrechet-Souza, L., Ceresér, K. M. M. & de Almeida, R. M. M. Microglial over-activation by social defeat stress contributes to anxiety- and depressive-Like behaviors. Front. Behav. Neurosci. 11, 207 (2017).

18. McKim, D. B. et al. Microglial recruitment of IL-1β-producing monocytes to brain endothelium causes stress-induced anxiety. Mol. Psychiatry 23, 1421-1431 (2018).

19. Milligan, E. D. & Watkins, L. R. Pathological and protective roles of glia in chronic pain. Nat. Rev. Neurosci. 10, 23-36 (2009).

20. Wang, X. et al. Morphine activates neuroinflammation in a manner parallel to endotoxin. Proc. Natl Acad. Sci. USA 109, 6325-6330 (2012).

21. Yang, Y. et al. Morphine promotes microglial activation by upregulating the EGFR/ERK signaling pathway. PLoS One. 16, e0256870 (2021).

22. Hutchinson, M. R. et al. Opioid-induced glial activation: mechanisms of activation and implications for opioid analgesia, dependence, and reward. ScientificWorldJournal 7, 98-111 (2007).

23. Hu, S., Sheng, W. S., Lokensgard, J. R. & Peterson, P.K. Morphine induces apoptosis of human microglia and neurons. Neuropharmacology 42, 829-836 (2002).

24. Xie, N. et al. Glycogen synthase kinase-3 and p38 MAPK are required for opioid-induced microglia apoptosis. Neuropharmacology 59, 444-451 (2010).

25. Heneka, M. T. et al. Neuroinflammation in Alzheimer's disease. Lancet Neurol. 14, 388-405 (2015).

26. Zheng, Z. H. et al. Neuroinflammation induces anxiety- and depressive-like behavior by modulating neuronal plasticity in the basolateral amygdala. Brain Behav. Immun. 91, 505-518 (2021).

27. Jian Luo, J. et al. Colony-stimulating factor 1 receptor (CSF1R) signaling in injured neurons facilitates protection and survival. J Exp Med. 210, 157-172 (2013).

28. Davis, S. M. & Pennypacker, K. R. The role of the leukemia inhibitory factor receptor in neuroprotective signaling. Pharmacol Ther. 183, 50-57 (2018).

29. Elmore, M. R. P. et al. Colony-stimulating factor 1 receptor signaling is necessary for microglia viability, unmasking a microglia progenitor cell in the adult brain. Neuron 82, 380-97 (2014).

30. Chao. M. V. Neurotrophins and their receptors: a convergence point for many signalling pathways. Nat. Rev. Neurosci. 4, 299-309 (2003).

31. Ghitza, U. E. Role of BDNF and GDNF in drug reward and relapse: a review. Neurosci. Biobehav. Rev. 35, 157-171 (2010).

32. Mazzon, C. et al. CCRL2 regulates M1/M2 polarization during EAE recovery phase. J. Leukoc Biol. 99, 1027–1033 (2016).

33. Müller, U., Bossy, B., Venstrom, K. & Reichardt, L. F. Integrin alpha 8 beta 1 promotes attachment, cell spreading, and neurite outgrowth on fibronectin. Mol. Biol. Cell 6, 433-448 (1995).

34. Ximerakis, M. et al. Single-cell transcriptomic profiling of the aging mouse brain. Nat. Neurosci. 22, 1696-1708 (2019).

35. Ammon-Treiber, S. et al. Rapid, transient, and dose-dependent expression of hsp70 messenger RNA in the rat brain after morphine treatment. Cell Stress Chaperones 9, 182-197 (2004).

36. Ammon, S., Mayer, P., Riechert, U., Tischmeyer, H. & Höllt, V. Microarray analysis of genes expressed in the frontal cortex of rats chronically treated with morphine and after naloxone precipitated withdrawal. Brain Res. Mol. Brain Res. 112, 113-125 (2003).

37. Nylandsted, J. et al. Heat shock protein 70 promotes cell survival by inhibiting lysosomal membrane permeabilization. J. Exp. Med. 200, 425-435 (2004).

38. Dorion, S. & Landry, J. Activation of the mitogen-activated protein kinase pathways by heat shock. Cell Stress Chaperones 7, 200-206 (2002).

39. O'Sullivan, S. J. et al. Single-cell glia and neuron gene expression in the central amygdala in opioid withdrawal suggests inflammation with correlated gut dysbiosis. Front. Neurosci. 13, 665 (2019).

40. Duan, K. et al. Mitophagy in the basolateral amygdala mediates increased anxiety induced by aversive social experience. Neuron 109, 3793-3809 (2021).

41. Hollis, F. et al. Mitochondrial function in the brain links anxiety with social subordination. Proc. Natl Acad. Sci. USA 112, 15486-15491 (2015).

42. Shahroodi, A. et al. Impact of different intensities of forced exercise on deficits of spatial and aversive memory, anxiety-like behavior, and hippocampal BDNF during morphine abstinence period in male rats. Metab. Brain Dis. 35, 135-147 (2020).

43. Zan, G. Y. et al. Amygdalar κ-opioid receptor-dependent upregulating glutamate transporter 1 mediates depressive-like behaviors of opioid abstinence. Cell Rep. 37, 109913 (2021).

44. Wu, Y. E., Pan, L., Zuo, Y., Li, X. & Hong, W. Detecting activated cell populations using single-cell RNA-seq. Neuron 96, 313-329 (2017).

45. Yang, Y. & Wang, J. Z. From structure to behavior in basolateral amygdala-hippocampus circuits front. Neural Circuits 11, 86 (2017).

46. Vickovic, S. et al. High-definition spatial transcriptomics for in situ tissue profiling. Nat. Methods 16, 987-990 (2019).

47. Taylor, J. R., Punch, L. J. & Elsworth, J. D. A comparison of the effects of clonidine and CNQX infusion into the locus coeruleus and the amygdala on naloxone-precipitated opiate withdrawal in the rat. Psychopharmacology 138, 133-142 (1998).

48. Zapala, M. A. et al. Adult mouse brain gene expression patterns bear an embryologic imprint. Proc. Natl Acad. Sci. USA 102, 10357-10362 (2005).

49. Saxena, A. et al. Trehalose-enhanced isolation of neuronal sub-types from adult mouse brain. Biotechniques 52, 381-385 (2012).

50. Satija, R., Farrell, J. A., Gennert, D., Schier, A. F. & Regev, A. Spatial reconstruction of single-cell gene expression data. Nat. Biotechnol. 33, 495-502 (2015).

675 51. Hao, Y. et al. Integrated analysis of multimodal single-cell data. Cell 184, 3573-3587 (2021).

676 52. Stuart, T. et al. Comprehensive integration of single-cell data. Cell 177, 1888-1902 (2019).

677 53. Marques, S. et al. Oligodendrocyte heterogeneity in the mouse juvenile and adult central
678 nervous system. Science 352, 1326–1329 (2016).

679 54. Hammond, T. R. et al. Single-cell RNA sequencing of microglia throughout the mouse
680 lifespan and in the Injured brain reveals complex cell-state changes. Immunity 50, 253-271
681 (2019).

682 55. Vanlandewijck, M. et al. A molecular atlas of cell types and zonation in the brain
683 vasculature. Nature 554, 475–480 (2018).

684 56. Tasic, B. et al. Adult mouse cortical cell taxonomy revealed by single cell transcriptomics.
685 Nat. Neurosci. 19, 335–346 (2016).

686 57. Jordao, M. J. C. et al. Single-cell profiling identifies myeloid cell subsets with distinct fates
687 during neuroinflammation. Science 363, 6425 (2019).

688 58. Kalish, B. T. et al. Single-cell transcriptomics of the developing lateral geniculate nucleus
689 reveals insights into circuit assembly and refinement. Proc. Natl Acad. Sci. USA 115, E1051-
690 E1060 (2018).

691 59. Zhang, Y. et al. An RNA-sequencing transcriptome and splicing database of glia, neurons,
692 and vascular cells of the cerebral cortex. J. Neurosci. 34, 11929-11947 (2014).

693 60. Han, X. et al. Mapping the mouse cell atlas by Microwell-Seq. Cell 172, 1091–1107.e1017
694 (2018).

695 61. Campbell, J. N. et al. A molecular census of arcuate hypothalamus and median eminence
696 cell types. Nat. Neurosci. 20, 484–496 (2017).

697 62. Llorens-Bobadilla, E. et al. Single-cell transcriptomics reveals a population of dormant neural
698 stem cells that become activated upon brain injury. Cell Stem Cell. 17, 329–340 (2015).

699 63. Liu, Y. et al. CD44 expression identifies astrocyte-restricted precursor cells. Dev. Biol. 276,
700 31–46 (2004).

701 64. Zeisel, A. et al. Brain structure. Cell types in the mouse cortex and hippocampus revealed by
702 single-cell RNA-seq. Science 347, 1138–1142 (2015).

703 65. Batiuk, M. Y. et al. Identification of region-specific astrocyte subtypes at single cell
704 resolution. Nat. Commun. 11, 1220 (2020).

705 66. Robinson, M. D., McCarthy, D. J. & Smyth, G. K. edgeR: a Bioconductor package for
706 differential expression analysis of digital gene expression data. Bioinformatics 26, 139-140
707 (2010).

708 67. Lun, A. T. L., Chen, Y. & Smyth, G. K. It's DE-licious: a recipe for differential expression
709 analyses of RNA-seq experiments using quasi-likelihood methods in edgeR. Methods in
710 Molecular Biology 1418, 391–416 (2016).

68. Soneson, C. & Robinson, M. D. Bias, robustness and scalability in single-cell differential expression analysis. Nat. Methods 15, 255-261 (2018).

69. Mootha, V. K. et al. PGC-1α-responsive genes involved in oxidative phosphorylation are coordinately downregulated in human diabetes. Nat. Genet. 34, 267-273 (2003).

70. Reimand, J. et al. Pathway enrichment analysis and visualization of omics data using g:Profiler, GSEA, Cytoscape and EnrichmentMap. Nat. Protoc. 14, 482–517 (2019).

71. Kucera, M., Isserlin, R., Arkhangorodsky, A. & Bader, G. D. AutoAnnotate: a Cytoscape app for summarizing networks with semantic annotations. F1000Research 5, 1717 (2016).

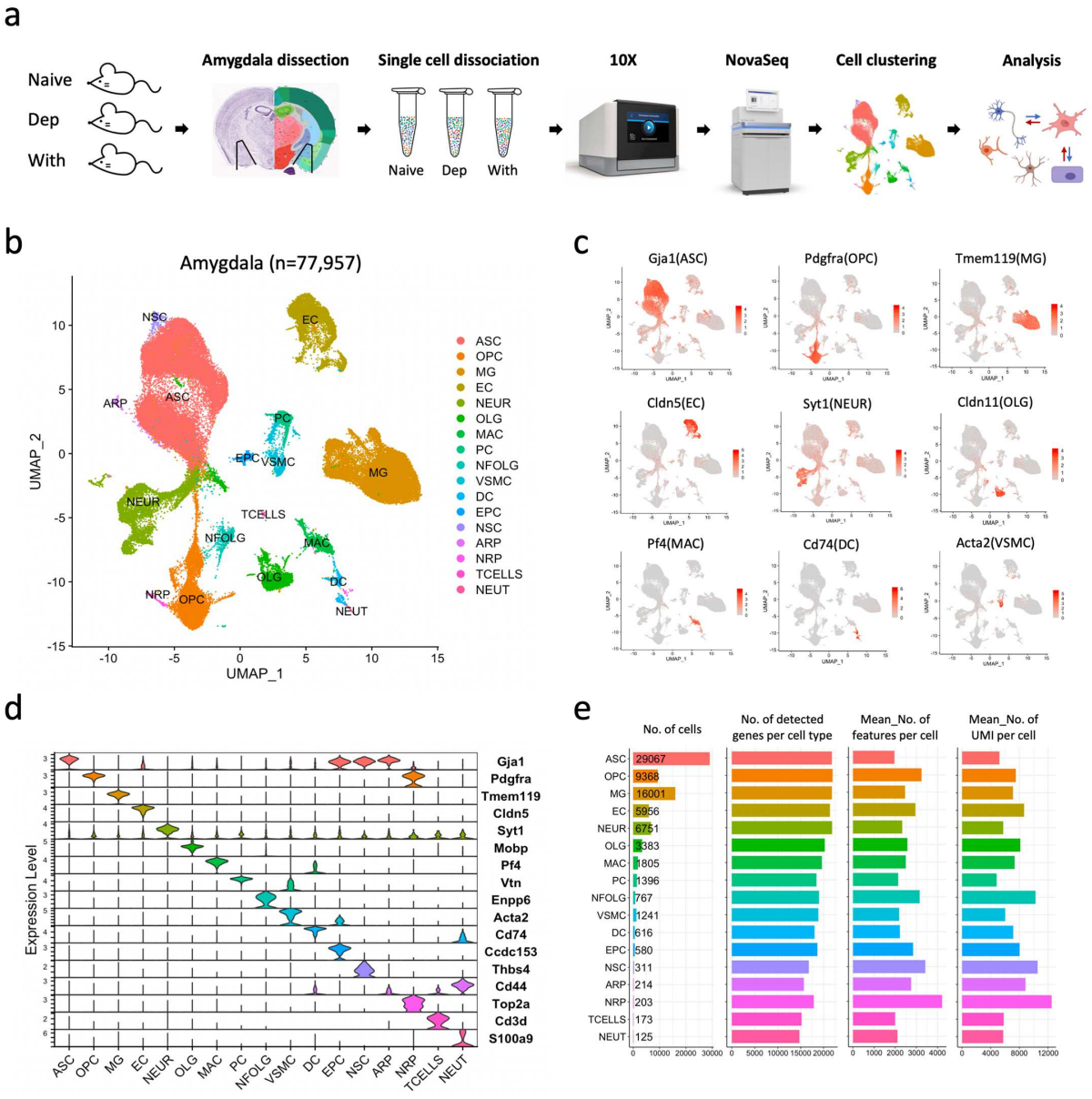

Fig.1 Identification of cell types in mouse amygdala. a, Schematic of the experimental workflow. Naive: naïve mice; Dep: mice under morphine dependence condition; With: mice under morphine withdrawal condition (see details in Supplementary Fig. 1a). **b,** UMAP (Uniform Manifold Approximation and Projection) plot showing the clustering of 77,957 cells (27141 from Naive, 27275 from Dep, 23541 from With) based on transcriptome. ASC, (astrocytes, *Gja1*$^+$), OPC (oligodendrocyte progenitor cells, *Pdgfra*$^+$), MG (microglial, *Tmem119*$^+$), EC (endothelial cells, *Cldn5*$^+$), NEUR (neurons, *Syt1*$^+$), OLG (oligodendrocytes, *Mobp*$^+$ or *Cldn11*$^+$), MAC (macrophages, *Pf4*$^+$), PC (pericytes, *Vtn*$^+$), NFOLG (newly-formed oligodendrocytes, *Enpp6*$^+$), VSMC (vascular smooth muscle cells, *Acta2*$^+$), DC (dendritic cells, *Cd74*$^+$), EPC (ependymocytes, *Ccdc153*$^+$), NSC (neural stem cells, *Thbs4*$^+$), ARP (astrocyte-restricted precursors, *Cd44*$^+$), NRP (neuronal-restricted precursors, *Top2a*$^+$), TCELLS (T cells, *Cd3d*$^+$) and NEUT (neutrophiles, *S100a9*$^+$). **c,** UMAP plots of 9 cell populations showing the expression of cell type-specific/enriched marker genes. **d,** Violin plot showing the expression of well-known cell type-specific/enriched marker genes in 17 cell clusters. **e,** Bar plots showing the number of cells, number of detected genes in each cluster, the average number of features (genes) and UMI counts in each cluster.

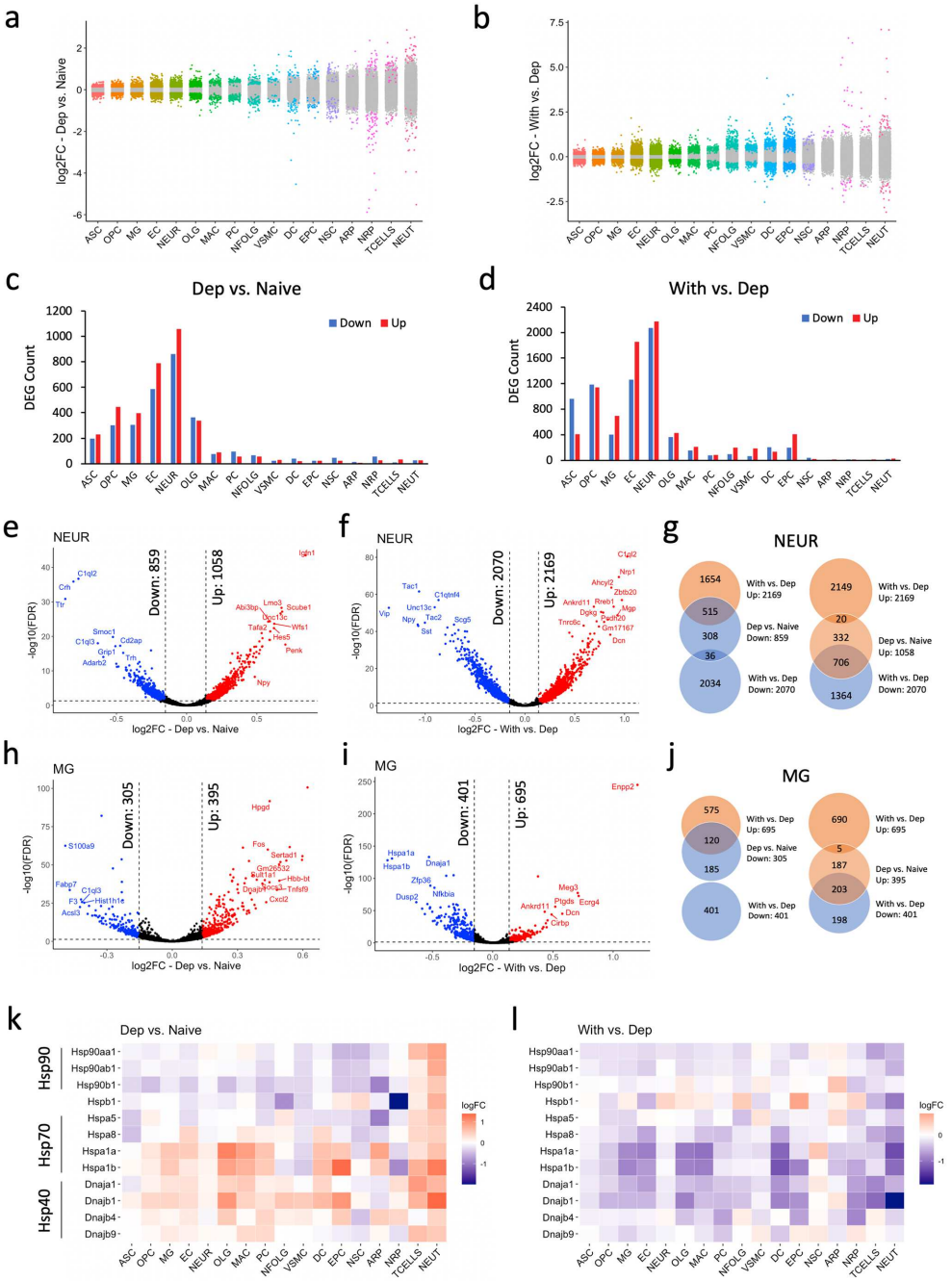

Fig.2 Differentially expressed genes under morphine dependence and withdrawal conditions. a, b, Strip charts showing the logarithmic fold changes (log2FC) of all detected genes (dots) in 17 clusters. Genes in colored dots are significantly changed (FDR < 0.05 and FC > 10%) comparing Dep to Naive (**a**), or With to Dep (**b**). **c, d,** Bar plots showing the number of significantly downregulated (Down) or upregulated (Up) genes in 17 clusters, comparing Dep to Naive (**c**), or With to Dep (**d**). **e, f,** Volcano plots showing the log2FC and -log10(FDR) of detected genes in NEUR, comparing Dep to Naive (**e**), or With to Dep (**f**). Significantly downregulated genes are dots in blue, upregulated genes are in red and genes in black are not significantly changed. **g,** Venn diagram showing the overlap of Dep vs. Naive upregulated genes (left) or downregulated genes (right) with With vs. Dep upregulated or downregulated genes in NEUR. **h, i,** Volcano plots showing the log2FC and -log10(FDR) of detected genes in MG, comparing Dep to Naive (**h**), or With to Dep (**i**). Significantly downregulated genes are dots in blue, upregulated genes are in red and genes in black are not significantly changed. **j,** Venn diagram showing the overlap of Dep vs. Naive upregulated genes (left) or downregulated genes (right) with With vs. Dep upregulated or downregulated genes in MG. **k, l,** Heatmaps showing the log2FC of heat shock protein expressions comparing Dep to Naive (**k**), or With to Dep (**l**) in 17 clusters.

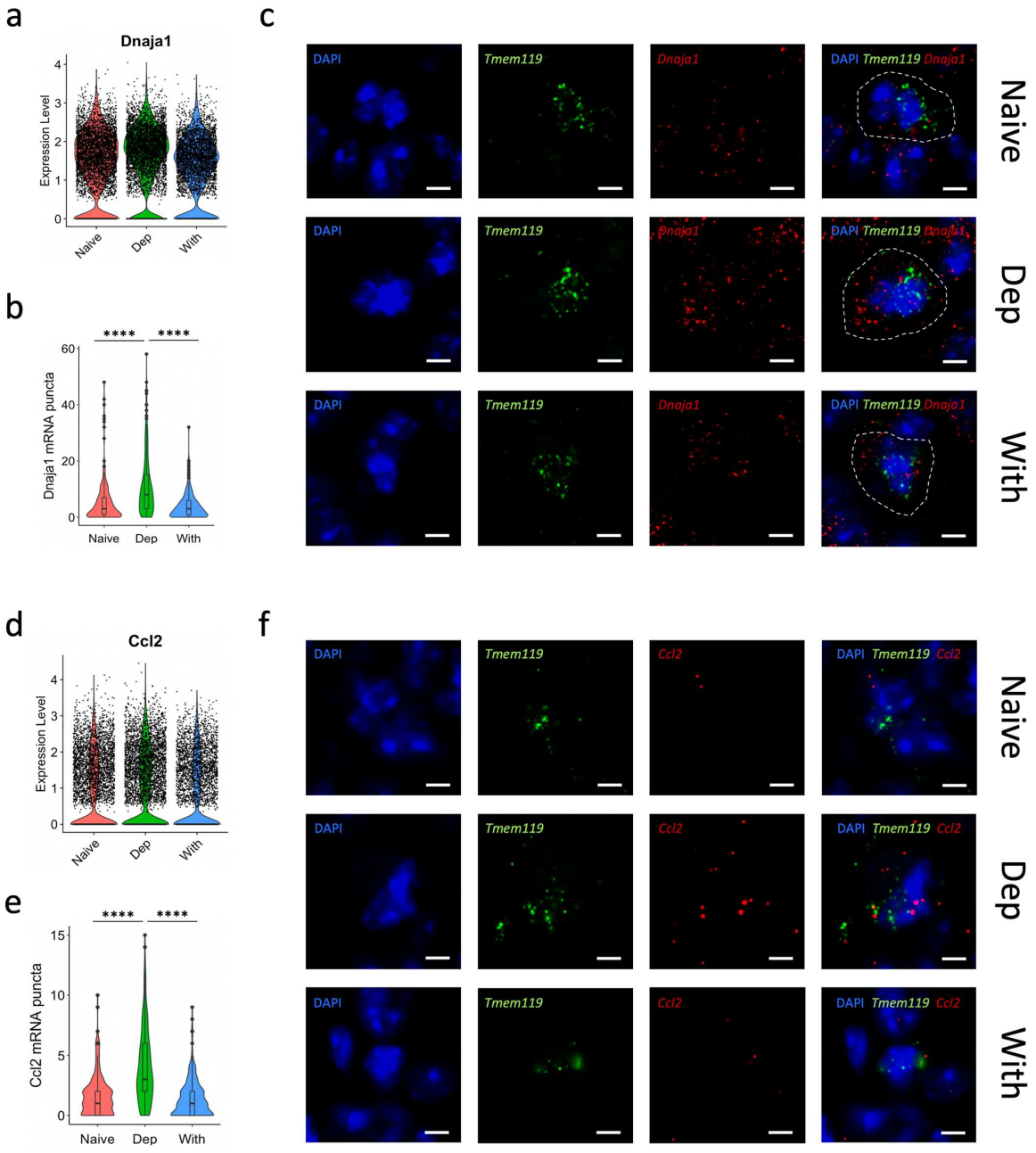

Fig. 3 Validation of heat shock protein gene and immune related gene expressions in MG. a, Violin plot overlaid with dot plot showing the expression levels of *Dnaja1* in our scRNA-seq data of MG population. **b,** Violin plot overlaid with box plot showing the quantification of the RNAscope data. Data represents median expression of *Dnaja1* (number of mRNA puncta) in *Tmem119*$^{+}$ MG cells (n=249 cells from 5 Naive mice, n=280 cells from 5 Dep mice, n=288 cells from 5 With mice). **** p value < 0.0001 by Mann-Whitney U-test. **c,** Representative RNAscope images of mouse amygdala showing the *Dnaja1* mRNA puncta in *Tmem119*$^{+}$ MG cells. Dotted lines outline the area of each cell that was considered for quantification. Scale bars, 5μm. **d,** Violin plot overlaid with dot plot showing the expression levels of *Ccl2* in our scRNA-seq data of MG population. **e,** Violin plot overlaid with box plot showing the quantification of the RNAscope data. Data represents median expression of *Ccl2* (number of mRNA puncta) in *Tmem119*$^{+}$ MG cells (n=291 cells from 5 Naive mice, n=303 cells from 5 Dep mice, n=313 cells from 5 With mice). **** p value < 0.0001 by Mann-Whitney U-test. **f,** Representative RNAscope images of mouse amygdala showing the *Ccl2* mRNA puncta in *Tmem119*$^{+}$ MG cells. Scale bars, 5μm.

a

NEUR - Dep vs. Naive

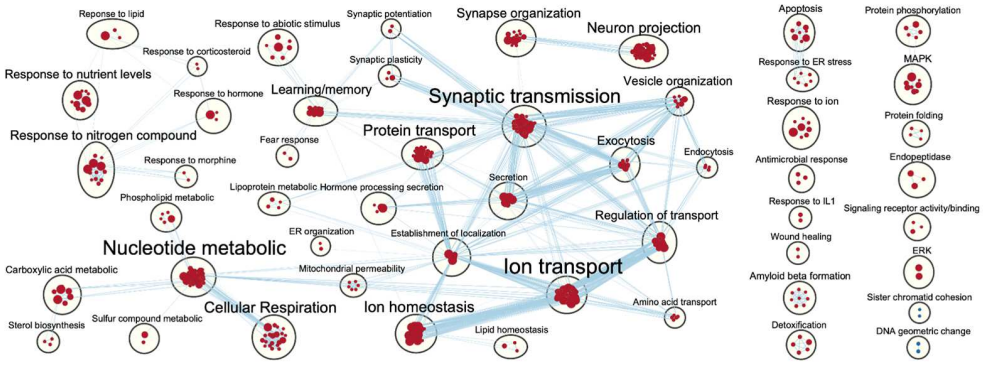

b

NEUR - With vs. Dep

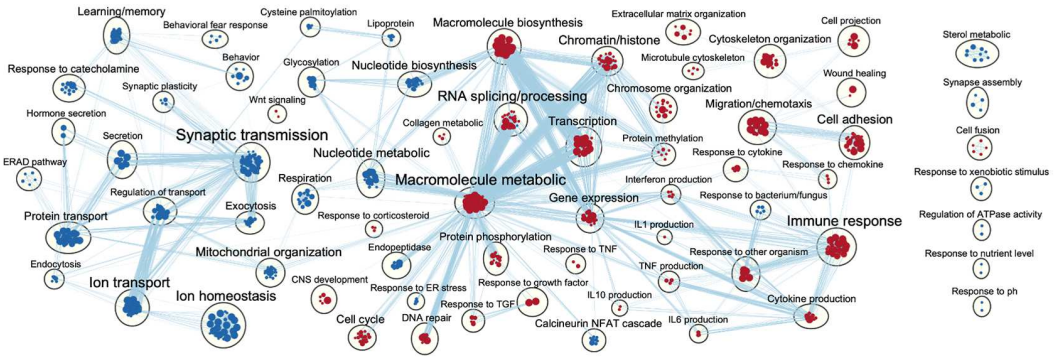

c

MG - Dep vs. Naive

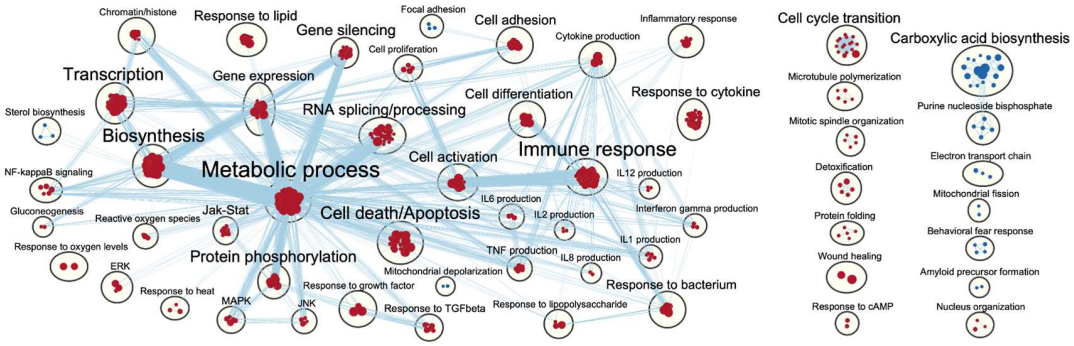

d

MG - With vs. Dep

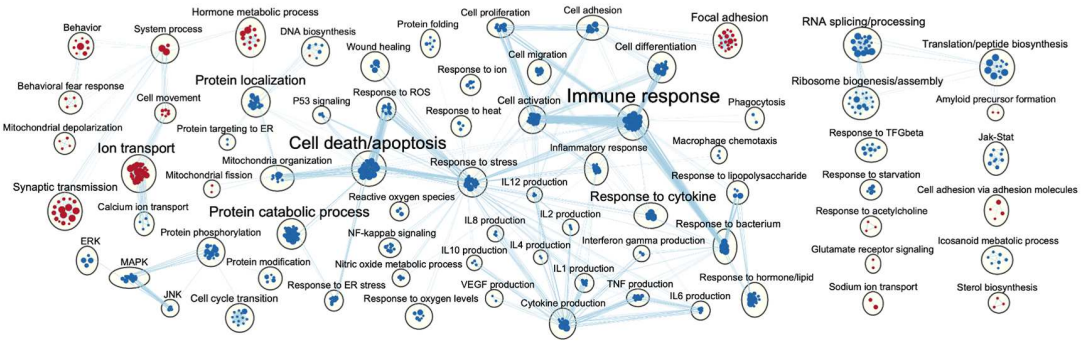

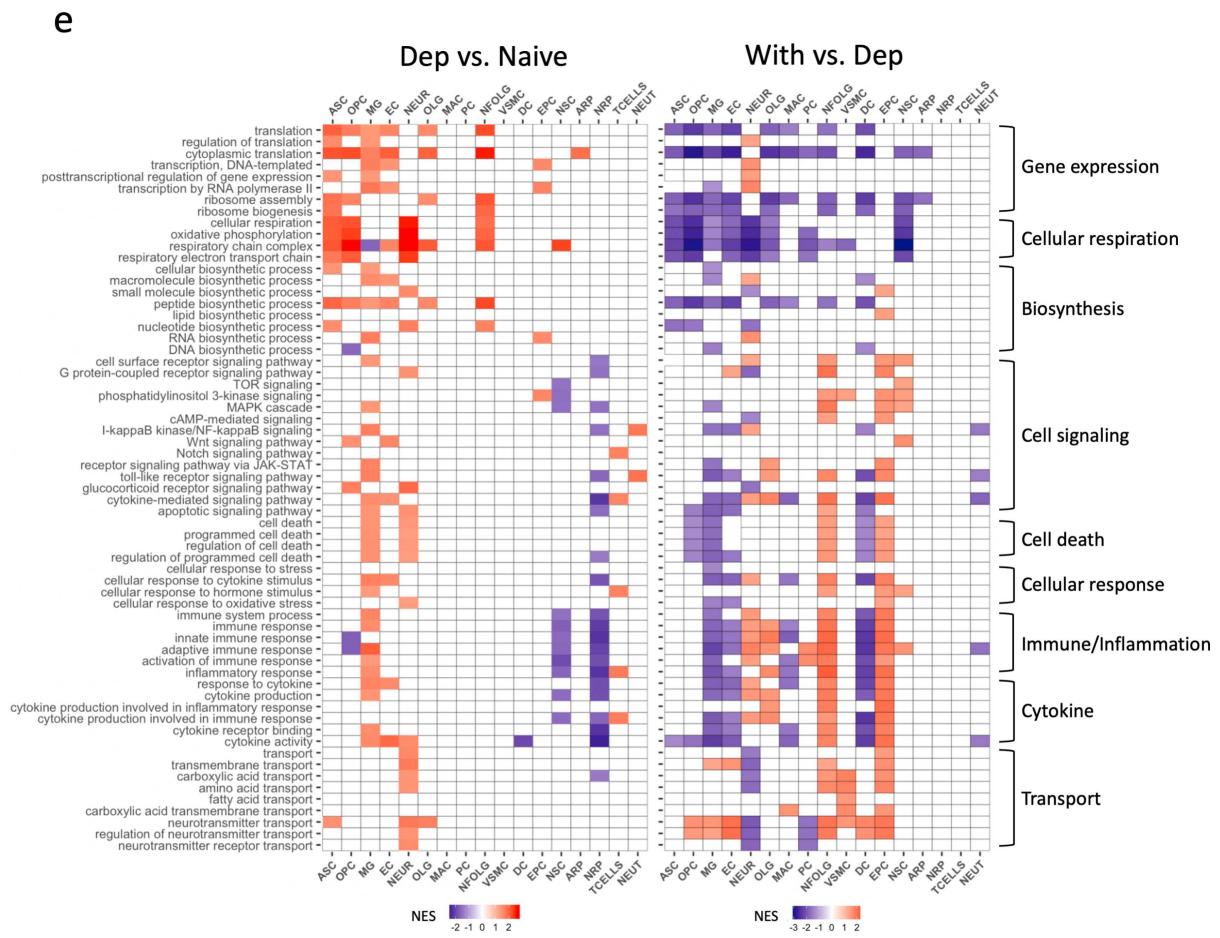

Fig. 4 Changes of biological pathways and processes under morphine dependence and withdrawal conditions. a, b, Enrichment maps of significant pathways (p value < 0.05 and FDR q value < 0.15) in NEUR comparing Dep to Naive (**a**), or With to Dep (**b**). Normalized enrichment scores (NES) were calculated for each pathway by GSEA (see Methods). The networks were created using EnrichmentMap Cytoscape application (see Methods). Pathways are shown as nodes which are colored by the corresponding NES, and edges represent the number of genes overlapping between two pathways. Clusters of nodes were labeled using the AutoAnnotate Cytoscape application to identify major biological themes. Positive NES (red nodes) indicate upregulation, while negative NES (blue nodes) indicate downregulation. **c, d,** Enrichment maps of significant pathways (p value < 0.05 and FDR q value < 0.15) in MG comparing Dep to Naive (**c**), or With to Dep (**d**). **e,** Heatmap of NES showing a subset of significant pathways (p value < 0.05 and FDR q value < 0.25) in 17 cell types comparing Dep to Naive (left), or With to Dep (right). Positive NES indicates upregulation, negative NES indicates downregulation and white indicates no significant change.

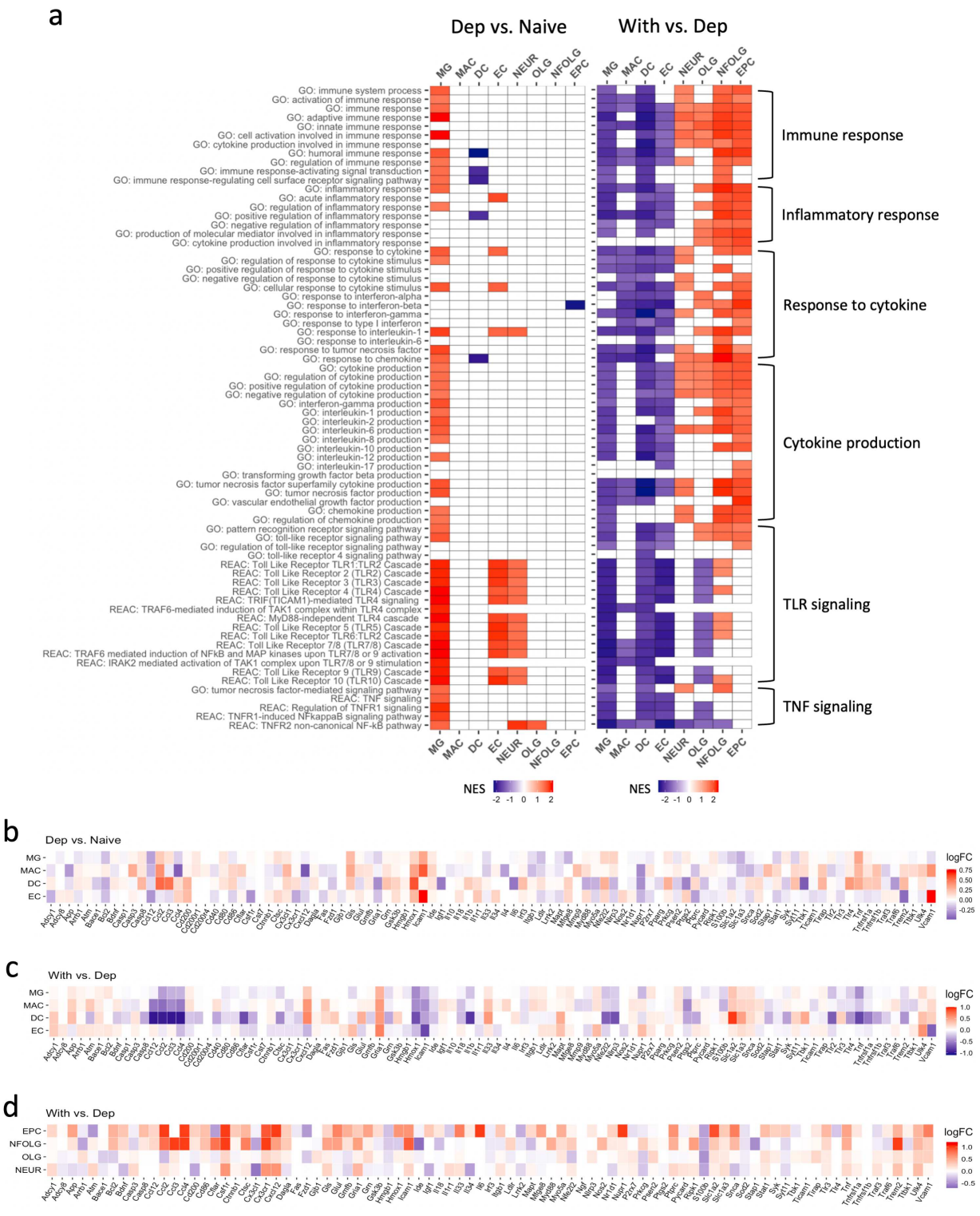

Fig. 5 Changes of immune/inflammation related pathways and genes under morphine dependence and withdrawal conditions. a, Heatmap of NES showing a subset of immune/inflammation related significant pathways (p value < 0.05 and FDR q value < 0.25) in 8 cell types comparing Dep to Naive (left), or With to Dep (right). Positive NES indicates upregulation, negative NES indicates downregulation and white indicates no significant change. **b,** Heatmap showing the log2FC of inflammation related gene expressions comparing Dep to Naive in MG, MAC, DC, EC. **c, d,** Heatmaps showing the log2FC of inflammation related gene expressions comparing With to Dep in MG, MAC, DC, EC (**c**), and in EPC, NFOLG, OLG, NEUR (**d**).

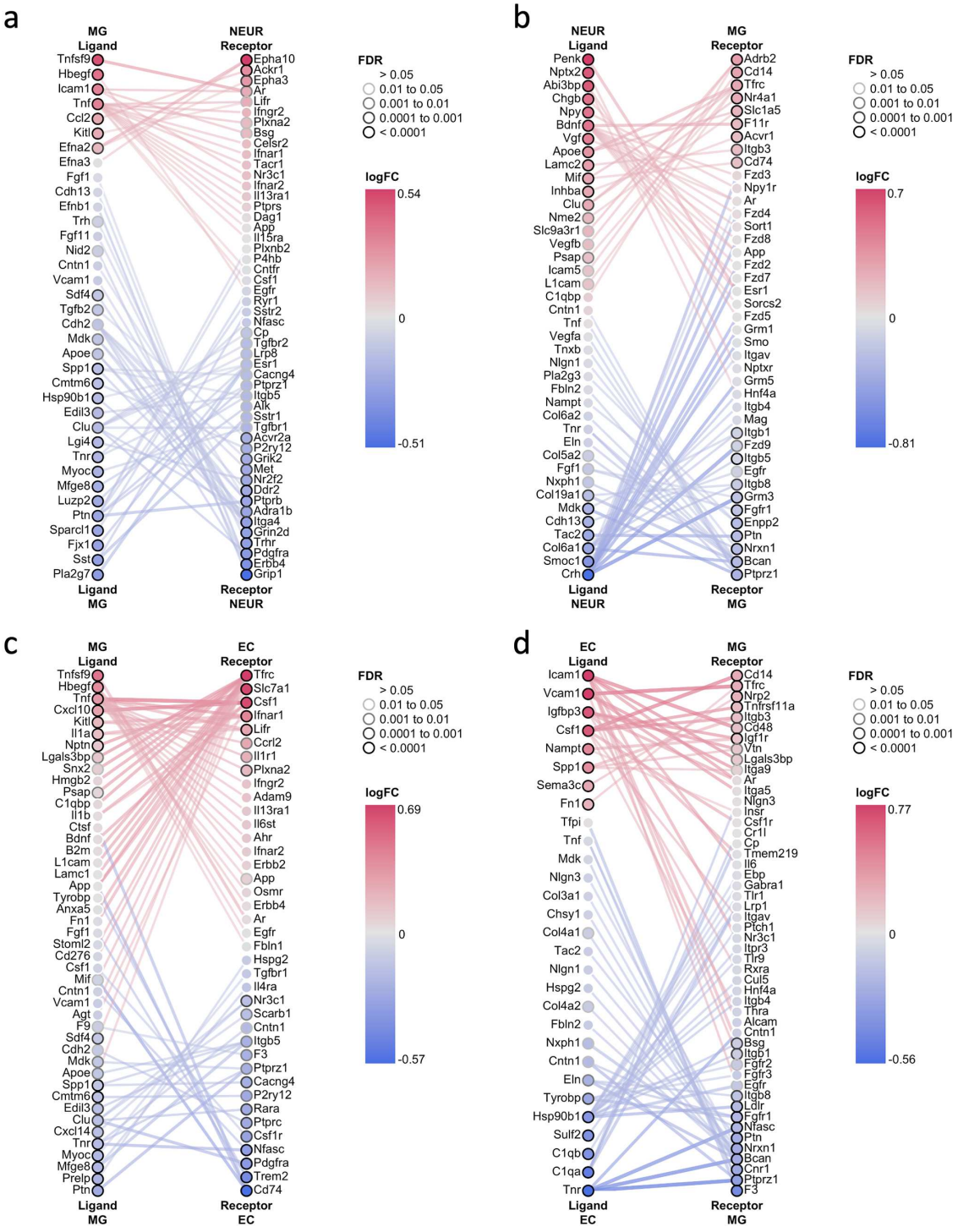

Fig. 6 Changes of cell-cell interactions with chronic morphine treatment. Ligands or receptors in the denoted cell type are represented by the nodes which are colored by the log2FC. Node borders indicate the FDR value of the DEG analysis. Edges represent ligand-receptor interactions. Edge color indicates the sum of scaled differential expression magnitudes from the ligand node and receptor node. The figures have been filtered so that the top 75 edges representing the most differentially expressed node pairs are shown. The comparisons were between Dep and Naive samples. **a,** ligands expressed in MG with receptors expressed in NEUR. **b,** ligands expressed in NEUR with receptors expressed in MG. **c,** ligands expressed in MG with receptors expressed in EC. **d,** ligands expressed in EC with receptors expressed in MG.

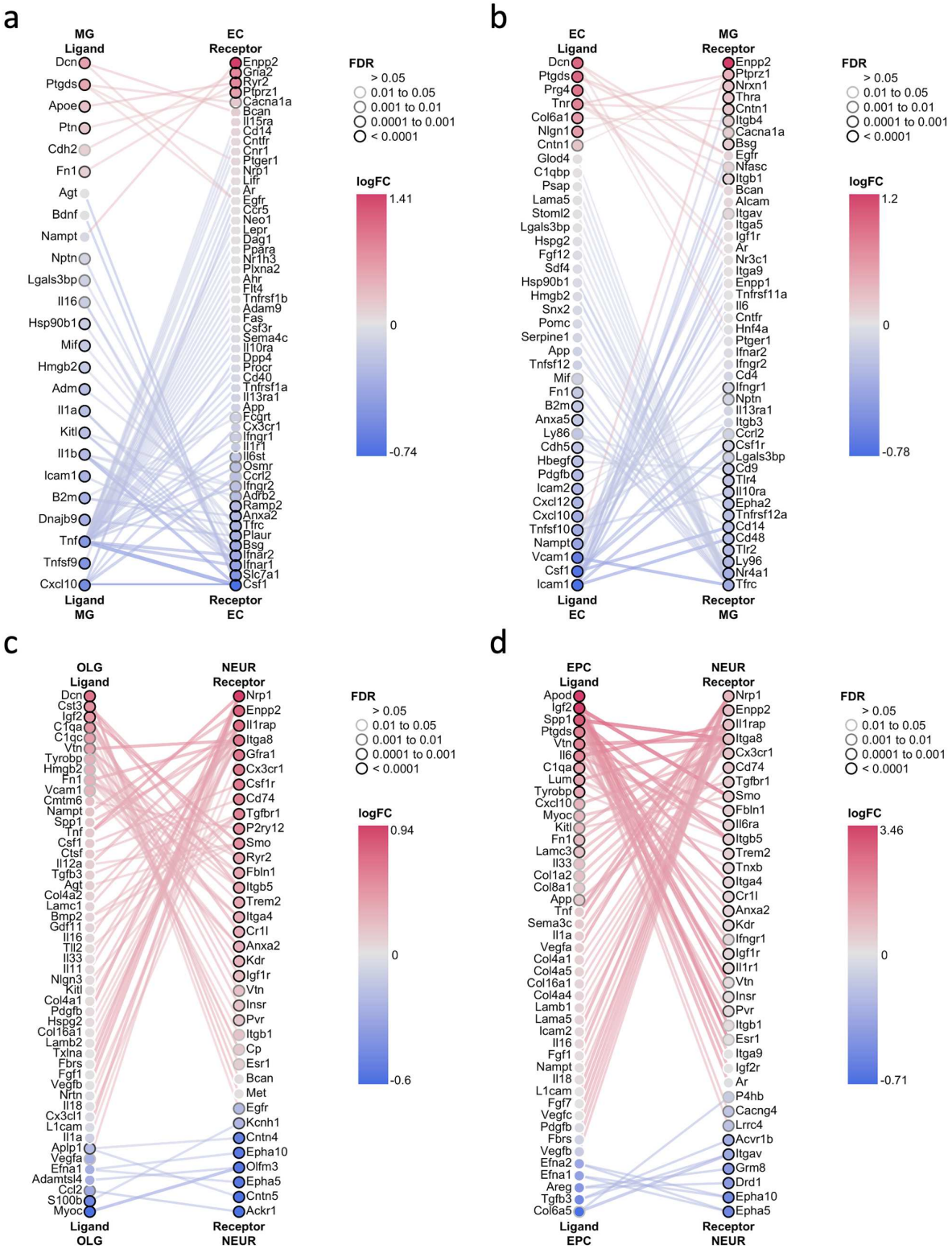

Fig. 7 Changes of cell-cell interactions during morphine withdrawal. The comparisons were between With and Dep samples. **a,** ligands expressed in MG with receptors expressed in EC. **b,** ligands expressed in EC with receptors expressed in MG. **c,** ligands expressed in OLG with receptors expressed in NEUR. **d,** ligands expressed in EPC with receptors expressed in NEUR.

Supplementary Files

This is a list of supplementary files associated with this preprint. Click to download.

- YanetalSupplementaryfigures.pdf